XVIII IMEKO WORLD CONGRESS
Metrology for a Sustainable Development
September, 17 – 22, 2006, Rio de Janeiro, Brazil

INDUCTIVE CONDUCTIVITY CELL FOR WATER SALINITY MONITORING

A. Lopes Ribeiro[1], *Helena M. Geirinhas Ramos*[1], *Pedro M. Ramos*[1] and *J.M. Dias Pereira*[1,2]

[1] Instituto de Telecomunicações, DEEC, IST, Av. Rovisco Pais, 1049-001, Lisboa, Portugal, arturlr@ist.utl.pt
[2] ESTSetúbal-LabIM/IPS, Rua do Vale de Chaves, Estefanilha, 2914-508 Setúbal, Portugal, joseper@est.ips.pt

Abstract: In this paper we describe an inductive sensor constructed as a double transformer, to be utilized to measure the water salinity in the sea and estuaries. The sensor uses two toroidal cores. Each core is provided with one single winding. The windings have equal number of turns. The electromotive forces developed in the water give rise to electrical currents which act as the secondary currents of one transformer and the primary currents of the other. Therefore, the relation between the voltage applied to the primary circuit and the voltage in the secondary depend on the conductivity of the water.

Keywords: inductive conductivity sensor, water conductivity, electrolytic conductivity, salinity.

1. INTRODUCTION

The salinity of the water on the open sea or inside estuaries, where the salty tide meets the fresh water current, may be measured by using conductivity sensors because the electric conductivity is directly related to the salt content in the water.

The growing attention on environmental issues fuelled the necessity of developing sensors to monitor the water quality. The need for permanent operation of the measurement apparatus poses a maintenance problem related to the continuous growing of biological organisms and to the continuous deposition of inorganic materials which foul the equipment and degrade the acquired data.

The utilization of nude electrodes is especially vulnerable to fouling, because the conductance between electrodes is very sensitive to the depositions on their surface.

The inductive sensors present the advantage of a non-direct contact between the sensor elements and the medium under test [1-3]. Therefore this type of sensors has been used in non-destructive tests to detect internal flaws inside mechanical structures [4], in non-invasive tests in biomedical applications [5] and in water conductivity assessment [1].

The basic principle involved in the inductive sensors consists in the presence of eddy currents induced in the interior of the body under test and due to the time variation of the magnetic flux originated by the electric currents imposed in a primary coil. The intensity of these currents is related to the electric conductivity of the medium and there is a correlation between the electrical parameters that can be assessed and the medium conductivity. In our sensor the electric current in the water provides the magnetomotive force necessary to magnetize a second ferromagnetic core, inducing a voltage in the secondary winding which is correlated to the conductivity of the water.

2. SENSOR DESIGN

The sensor structure is shown in Fig. 1. Two toroidal cores of amorphous iron are mounted together as shown in Fig. 1. Each core is provided with one winding of 20 turns. This assemble is immersed in the aqueous solution. A plastic container is used to delimit the lines of current inside the water, preventing the influence of strange objects on the measuring process. Therefore all the current in the water is enclosed by the plastic container. However, the container is provided with some apertures to let the water flow through the cell. The expected lines of current are depicted in the Fig. 2.

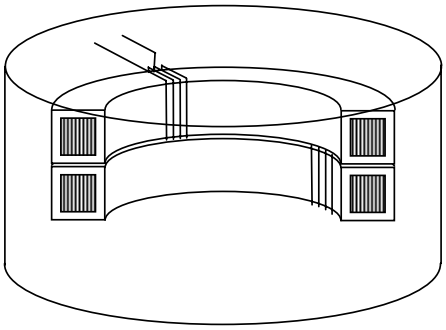

Fig. 1 Cell structure: two cores with one winding each inside a plastic container.

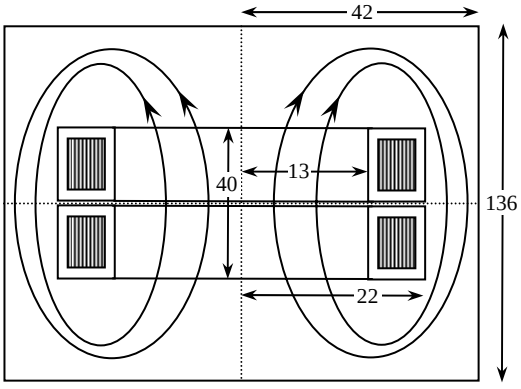

Fig. 2 Lines of current embracing the two toroids inside the plastic container. The dimensions are in millimeters.

The cell will work in an alternate sinusoidal regime. However, the resistance of the water path may be calculated

assuming stationary fields, if the depth of penetration δ in the water is much greater than the cell dimensions for the maximum frequency of operation. Considering the maximum frequency as $f_{\max} = 50$ kHz and $\sigma_{\max} = 5$ S/m we obtain using (1), a value for the depth of penetration of the order of one meter. This will guarantee that the depth of penetration of the electromagnetic field in the salty water will always be greater than the dimensions of the sensor, for the entire range of the conductivities to be measured.

$$\delta_{\min} = \frac{2}{\sqrt{\omega_{\max}\mu_0\sigma_{\max}}} \tag{1}$$

2.1. Sensor Modeling

The finite element method was used to estimate the configuration of the electric field induced inside the cell. As shown in the previous section the current field can be determined as in the dc-regime. Equipotentials and lines of current were determined using this method. The lines of current are shown in the Fig. 3. These results allow the determination of the water resistance and of the cell constant. This modeling shows that the resistance R_W of the water path may be written in the form,

$$R_W = \frac{K_C}{\sigma} \tag{2}$$

where K_C is the cell constant, which only depends on the geometric shape. In our case and for the linear dimensions presented on the Fig. 2 the value K_C=110 m^{-1} was obtained.

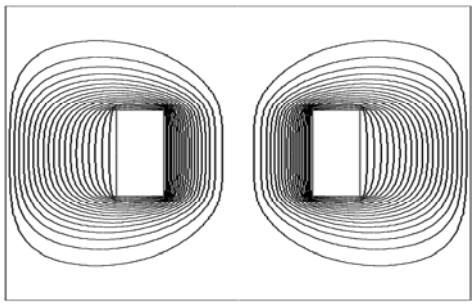

Fig. 3 Current lines obtained using the finite element method.

The electric circuit represented in Fig. 4 is useful to preview the electric behavior of the presented sensor. However in this scheme the dispersion of the magnetic field lines and the resistance of the wire windings are neglected. The effect of parasitic capacitances is not taken into account.

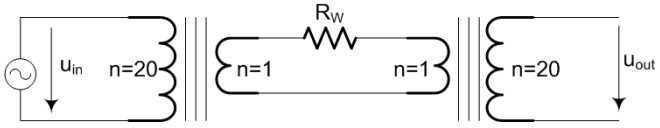

Fig. 4 Sensor schematic circuit: R_W represents the resistance of the water circuit.

The circuit represented in Fig.4 has an equivalent as represented in Fig.5. The first transformer is represented by the electric circuit as seen from the primary (the winding of 20 turns) and the second transformer as seen from the secondary (20 turns output). In this equivalent circuit $\bar{Z}$ represents the impedance of the 20 coils around one toroidal core. It was verified by measurement that, at the frequency of 50 kHz, the impedance $\bar{Z}$ presented an important real part with an angle of losses greater than $\pi/4$. However, the frequency of 50 kHz was chosen because the sensibility increases with frequency. It was also verified that the impedance $\bar{Z}$ did not present important variations for input amplitude voltage variations between 5 and 10 volt.

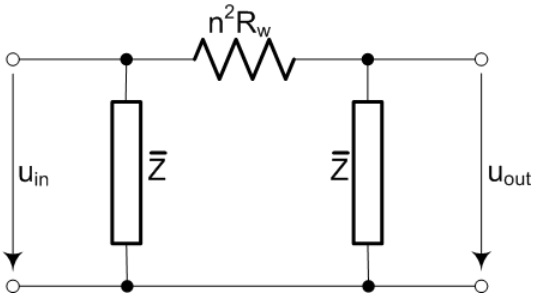

Fig. 5 Equivalent circuit of the double transformer sensor.

With this model it was possible to preview the behavior of the sensor when it was driven by a constant voltage source or when it was driven by a constant current source. For a voltage of imposed constant amplitude applied to the input transformer the expected output voltage phasor will be

$$\bar{U}_{out} = \bar{U}_{in}\frac{\bar{Z}}{\bar{Z} + n^2 R_W}. \tag{3}$$

A close examination of the expression (3) shows that the expected sensitivity of the output voltage to the water resistance R_W varies largely in the range of measurement:

$$\left|\frac{d\bar{U}_{out}}{dR_W}\right| = \left|\frac{-\bar{Z}n^2\bar{U}_{in}}{(\bar{Z} + n^2 R_W)^2}\right|. \tag{4}$$

Being the range of the conductivity measurement $(100\ \text{mS/m} < \sigma < 5\ \text{S/m})$, and taking the equation (2) into account, the corresponding values of the water resistance R_W will be in the interval $(1.1\ \text{k}\Omega > R_W > 22\ \Omega)$. For $\bar{Z} = (3.2\angle 37°)\ \text{k}\Omega$ and $\left|\bar{U}_{in}\right| = 1$ V, the sensitivity given by (4) will be in the interval

$$6{,}54\times10^{-6} < \left|\frac{d\bar{U}_{out}}{dR_W}\right| < 9{,}64\times10^{-3}\ \text{V/}\Omega \tag{5}$$

The sensitivity of the output voltage to the conductivity σ, also for unitary input voltage, will be given by

$$\left|\frac{d\bar{U}_{out}}{d\sigma}\right| = \left|\frac{d\bar{U}_{out}}{dR_W}\frac{dR_W}{d\sigma}\right| \tag{6}$$

which corresponds to the interval

$$72 > \left|\frac{d\bar{U}_{out}}{d\sigma}\right| > 42\ \text{mV/(S/m)}. \tag{7}$$

These results show that the expected absolute errors inherent to the sensor are of the same order of magnitude, for low or high conductivities, but quite different in relative value. Therefore a special attention must be taken when projecting the electronic circuitry associated to the detection of the sensor output voltage.

The sensor is driven by a sinusoidal oscillator working at f=50 kHz and rms output voltage of U_{out}=10 V. The components in phase and in quadrature of the sensor output voltage were measured separately. For a circuit with the topology of that shown in Fig.5, and for the values of $\bar{Z}$ and U_{out} referred above, the output sensor voltage components will vary with R_W as shown in the Fig.6.

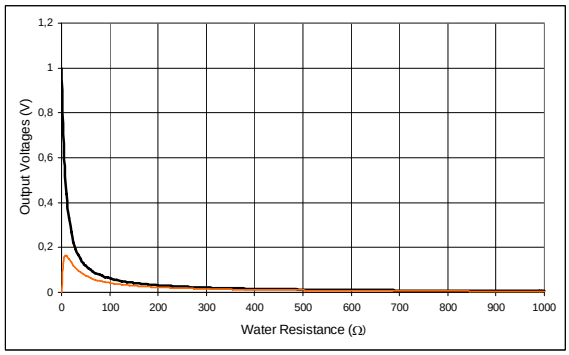

Fig. 6 Cell output voltage. The upper curve is the component in phase and the lower curve the component π/2 out of phase with the sensor input.

3. EXPERIMENTAL CHARACTERIZATION

The cell was characterized in a bath of salty water by using an automated set-up previously developed [6]. The cells were tested varying the frequency and the temperature, in baths of different salinities. Some of the obtained results are presented in Fig.7. These results show the dependence of the trans-impedance on the frequency, and were used to select the final frequency of operation for the prototype.

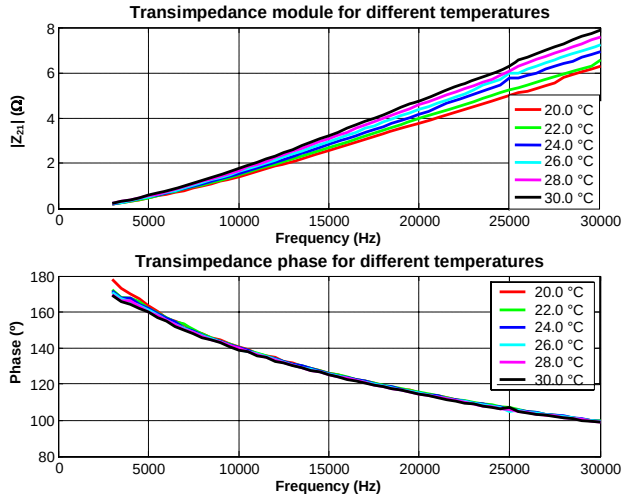

Fig. 7 Cell transimpedance as a function of frequency and temperature. The measurements correspond to a solution with conductivity of 43 mS/m at 20.0 ºC.

Fig.7 shows clearly that the sensitivity increases with the frequency. These measurements were carried out in a bath with conductivity lower than the minimum conductivity of the measurement range. For this low conductivity value it was possible to separate the curves measured for different temperatures, and confirm the theoretical law of variation with the temperature.

$$\sigma(T) = \sigma(T_0) \times \left[1 + \alpha(T - T_0)\right] \quad (8)$$

It was obtained for α the value of α=2.2%/ºC. This result allows that the conductivity measured values, for the sake of comparison, are converted to the same reference temperature.

4. BASIC ELECTRIC CIRCUITRY

In Fig.8 we represent a block diagram of the constructed circuitry for driving the sensor and to measure the output voltage, obtaining the components in phase and in quadrature with the input. For this purpose we utilized two integrated multipliers which incorporate low-pass filters necessary to extract the amplitudes of those components.

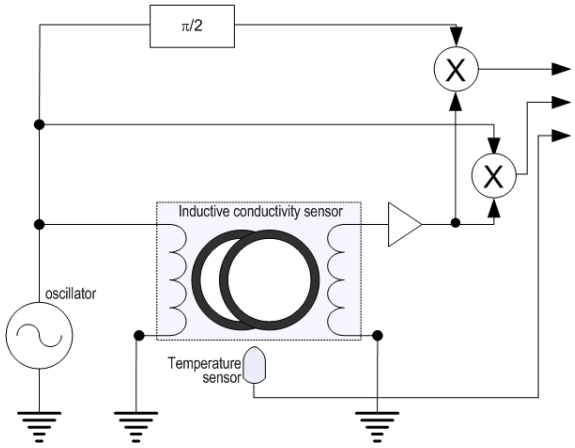

Fig. 8 Block diagram of the circuitry to obtain the components in phase and π/2 out of phase with the sensor input voltage.

The experimental values, obtained by using the set-up described in Fig. 8 are presented in Fig. 9 and show that, for the lower values of water conductivity, the output voltages are small. However the experimental points are in good agreement with the theoretical curve, presented above in Fig. 6.

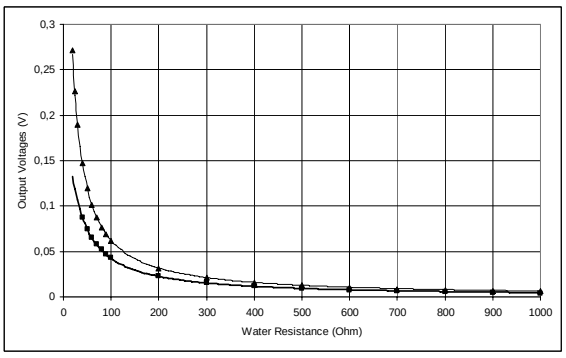

Fig. 9 The two components of the output voltage as a function of the water resistance R_W. In phase experimental values are marked with triangles and squares represent the quadrature component.

In Fig. 10 we present the experimental values of water conductivity as a function of the expected values, for a set of points marked with squares. These experimental points were obtained comparing, for a given value of water resistance the experimental values of the measured output voltages to

the values which were expected from the theoretical model presented above.

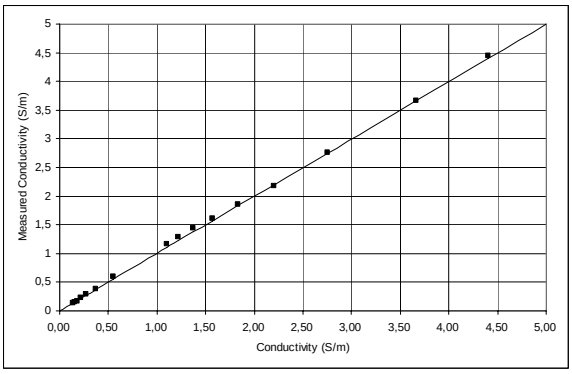

Fig. 10 Comparison of the obtained values of water conductivity to the theoretical values expected from the presented model.

4. CONCLUSION

An inductive conductivity cell to measure the electrical conductivity of the salty water was modeled, constructed and characterized in our laboratory. A number of these sensors will be placed in the river Tagus estuary near Lisbon. The array of sensors will work autonomously. Each sensor will be provided with a microprocessor to automate the measuring process and to control the transmission of data to a central point where the collected information will be processed. A second phase of this work is now in development. Meanwhile, a more complete characterization and comparison with other conductivity cells is underway.

ACKNOWLEDGMENTS

This work was supported in part by Portuguese Science and Technology Foundation (Fundação para a Ciência e Tecnologia). This support is gratefully acknowledged. We also acknowledge the Vacuumschmelz Company for providing the ferromagnetic cores.

REFERENCES

[1] K. Striggow, R. Dankert, “The exact theory of inductive conductivity sensors for oceanographic applications”, IEEE Journal of Oceanic Engineering, Vol. 10, N. 2, pp. 175-179, April 1985.

[2] A. J. Fougere, “New non-external field inductive conductivity sensor (NXIC) for long term deployments in biologically active regions”, OCEANS 2000 MTS/IEEE Conference and Exhibition, Vol. 1, pp. 623-630, Sept. 2000.

[3] A. Fougere, M. St Germain, F.J. Kelly, “Field evaluation of a revolutionary CTD design”, OCEANS 2003 Proceedings, Vol. 4, pp. 2249-2253, Sept. 2003.

[4] G. Miller, P. Gaydecki, S. Quek, B. T. Fernandes and M. A.M. Zaid, “Detection and imaging of surface corrosion on steel reinforcing bars using a phase-sensitive inductive sensor intended for use with concrete”, NDT & E International, Vol. 36, Issue 1, pp. 19-26, January 2003.

[5] L. W. Hart, H. W. Ko, J. H. Meyer Jr.; D. P. Vasholz, R. I. Joseph, “A noninvasive electromagnetic conductivity sensor for biomedical applications”, IEEE Transactions on Biomedical Engineering, Vol. 35, N. 12, pp. 1011-1022, Dec. 1988.

[6] Helena Ramos, Francisco Assunção, A. L. Ribeiro, Pedro Ramos, “A Low-Cost Temperature Controlled System to Test and Characterize Sensors”, Proceedings of the 10th IEEE Africon Conference, Vol. 01, pp. 57-60, Gaborone, Botswana, Sept. 2004.